Radiotherapy Decreases Vascular Density and Causes Hypoxia with Macrophage Aggregation in TRAMP-C1 Prostate Tumors

Fang-Hsin Chen,[1,2] Chi-Shiun Chiang,[1] Chun-Chieh Wang,[2,4] Chien-Sheng Tsai,[2,4] Shih-Ming Jung,[3] Chung-Chi Lee,[4] William H. McBride,[5] and Ji-Hong Hong[2,4]

Abstract

Purpose: To investigate how single or fractionated doses of radiation change the microenvironment in transgenic adenocarcinoma of the mouse prostate (TRAMP)-C1 tumors with respect to vascularity, hypoxia, and macrophage infiltrates.

Experimental Design: Murine prostate TRAMP-C1 tumors were grown in C57BL/6J mice to 4 mm tumor diameter and were irradiated with either 25 Gy in a single dose or 60 Gy in 15 fractions. Changes in vascularity, hypoxia, and macrophage infiltrates were assessed by immunohistochemistry and molecular assays.

Results: Tumor growth was delayed for 1 week after both radiation schedules. Tumor microvascular density (MVD) progressively decreased over a 3-week period to nadirs of 25% and 40% of unirradiated tumors for single or fractionated treatment, respectively. In accord with the decrease in MVDs, mRNA levels of endothelial markers, such as *CD31*, *endoglin*, and *TIE*, decreased over the same time period after irradiation. Central dilated vessels developed surrounded by avascularized hypoxic regions that became infiltrated with aggregates of CD68+ tumor-associated macrophages, reaching a maximum at 3 weeks after irradiation. Necrotic regions decreased and were more dispersed.

Conclusion: Irradiation of TRAMP-C1 tumors with either single or fractionated doses decreases MVD, leading to the development of disperse chronic hypoxic regions, which are infiltrated with CD68+ tumor-associated macrophages. Approaches to interfere in the development of these effects are promising strategies to enhance the efficacy of cancer radiotherapy.

The probability of local tumor control following radiation therapy (RT) is determined primarily by the number of clonogens (1, 2), their intrinsic cellular radioresistance, and microenvironmental factors, such as hypoxia, which are in turn dependent on tumor microvascularity (3). It has been reported that RT decreases the number of capillary-like structures formed by endothelial cells *in vitro* (4) and induces endothelial cell apoptosis in tumors *in vivo* (5). These cellular effects are thought to result in morphologic and functional changes in tumor vasculature after RT, which include degradation of the vascular wall, disruption of the endothelial lining, perivascular fibrosis, interstitial edema, and vasodilatation (6).

The link between vascular damage and effectiveness of tumor RT has been illustrated by animal models with the use of acid sphingomyelinase–deficient and Bax-deficient mice (7), in which tumors show less endothelial apoptosis after large single doses of irradiation and faster growth than in wild-type mice. There is, however, controversy about the importance of vascular damage in tumors receiving fractionated RT (8, 9).

Vascular function seems largely under the control of cytokines in the tumor microenvironment. The major sources of such cytokines are tumor-associated macrophages (TAM; ref. 10). Two distinct macrophage phenotypes, M1 or M2, have been described with the abilities to inhibit or promote tumor growth, respectively. The M1 phenotype is proinflammatory with high levels of inducible nitric oxide synthase production. The M2 phenotype (11) is anti-inflammatory, proangiogenic (12, 13), and promotes metastasis (14, 15). M1 and M2 TAMs seem to segregate to different areas of the tumor, with M2 TAMs migrating to and aggregating in avascular or hypoxia regions (16, 17). Surface markers that can distinguish M1 from M2 TAMs are still poorly defined, but F4/80 (18) or CD68 (17, 19) primarily identify M2 cells, with the two classes often being additionally defined by a composite of differences in scavenger

Authors' Affiliations: [1]Department of Biomedical Engineering and Environmental Sciences, National Tsing Hua University, Hsinchu, Taiwan; Departments of [2]Radiation Oncology and [3]Pathology, Chang Gung Memorial Hospital-LinKou and [4]Department of Medical Imaging and Radiological Science, Chang Gung University, Taoyuan, Taiwan; and [5]Roy E. Coats Research Laboratories, Department of Radiation Oncology, University of California at Los Angeles, Los Angeles, California
Received 6/5/08; revised 11/10/08; accepted 11/14/08.

Grant support: National Science Council, Taiwan, grant 96-2628-B-182-021-MY2, and Chang Gung Memorial Hospital grants CMRPG34025 and CMRPG360991; National Tsing Hua University, Taiwan, grant 96N2426E1 and National Science Council, Taiwan, grant 97-2314-B-007-003-MY2 (C-S. Chiang); and NIH/National Cancer Institute grant RO1 CA-101752 and Department of Defense grant W81XWH-04-1-0126 (W.H. McBride).

The costs of publication of this article were defrayed in part by the payment of page charges. This article must therefore be hereby marked *advertisement* in accordance with 18 U.S.C. Section 1734 solely to indicate this fact.

Note: Supplementary data for this article are available at Clinical Cancer Research Online (http://clincancerres.aacrjournals.org/).

Requests for reprints: Ji-Hong Hong, Department of Radiation Oncology, Chung Gung Memorial Hospital-Linkou, 5 Fu-Shin Street, Kwei-Shan, Taoyuan, Taiwan. Phone: 886-3-3282177; Fax: 886-3-3280797; E-mail: jihong@adm.cgmh.org.tw.

doi:10.1158/1078-0432.CCR-08-1471

Translational Relevance

Although reoxygenation is believed to confer a therapeutic advantage for fractionated radiotherapy (RT) of tumors, our animal model suggests that both single and fractionated RT may cause chronic and persistent hypoxia. Indeed, there seems to be a shift from transient to chronic hypoxia during the later times of a fractionated course of RT that is associated with aggregation of CD68+ tumor-associated macrophages in hypoxic regions. These phenomena are important for our understanding of how the tumor microenvironment changes during and after RT, and provide clues about potential targets for intervention to enhance the effectiveness of RTor to treat recurrent tumors.

receptor expression, effector function, and cytokine or chemokine production (11, 20).

The potential of RT to alter TAM phenotype and function has rarely been studied. In our previous study, TAMs isolated from irradiated tumors expressed higher arginase I, cyclooxygenase-2, and inducible nitric oxide synthase levels than those from unirradiated tumors and were more effective at promoting tumor growth (21). In this study, we further analyze the dynamic relationships among tumor vascularity, hypoxia, and TAMs in tumors regrowing during or after multifraction (MF) or single-dose (SD) RT, respectively.

Materials and Methods

Tumor model and tumor irradiation. All experiments were done with the use of 7-to-8-wk-old male C57BL/6J mice. The transgenic adenocarcinoma of the mouse prostate (TRAMP)-C1 prostate cancer cell line was derived from transgenic mice with adenocarcinoma of the mouse prostate (22) and was purchased from the ATCC (CRL-2730). Tumors were generated by i.m. inoculation of 3×10^6 viable cells into the thigh. Mice with tumors 4 mm in diameter were selected and randomly allocated to groups for experimentation [tumor diameter was defined as (a+b)/2, where a and b are the width of two dimensions of the mouse thigh] that contained at least 5 mice per time point.

The irradiation protocol was previously described (21), and tumors were irradiated with either a single dose of 25 Gy (SD) or 60 Gy in 15 fractions, 4 Gy per day and 5 d per week. The tumors were removed at indicated times after irradiation.

For detecting hypoxia, pimonidazole hydrochloride (Hypoxyprobe-1 Kit; Chemicon) was administered as 4 mg in 0.1 mL by i.v. injection. One hour after administration of the hypoxia marker, perfusion levels were determined by injecting mice i.v. with a 0.05-mL solution of Hoechst 33342 (Invitrogen) in PBS (pH 7.4) at a dose of 15 mg/kg. One minute after Hoechst injection, the mice were sacrificed, and the tumors were removed and stored in optimal cutting temperature compound at -80°C. During the experiments, all mice were cared for in accordance with the guidelines approved by the Commission of Chinese National Laboratory Animal (approval number CGU03-59).

RNA isolation and RNase protection assay. The technique has been described in detail elsewhere (23). A set of mAngio-1 Multi-Probe Template (BD Biosciences) was used for RNase protection assay. The gel of the RNase protection assay samples in the same plate was exposed to film for various times to acquire adequate signal intensity appropriate for each gene, and the optical density of each band was determined by the free software ImageJ (http://rsb.info.nih.gov/ij/). The expression level of mRNA of each gene was normalized to the housekeeping gene, L32, and the ratio of expression to the control at 0 h was calculated.

Immunohistochemistry. Ten-micrometer cryostat sections were fixed in methanol at -20°C for 10 min and then rehydrated in PBS. Nonspecific binding was blocked by incubating sections in 1% bovine serum albumin in PBS for 30 min. Tumor sections were double stained for pimonidazole in combination with *CD31* or CD68. Pimonidazole was detected with mouse antibody (Chemicon) and goat anti-mouse IgG-γ1 Alexa 488 (Invitrogen). For verification of chronic hypoxic cells, the section adjacent to that used for pimonidazole staining was stained with goat anti–carbonic anhydrase IX antibody (R&D Systems Inc.) and donkey anti-goat IgG Cy3 antibody (Chemicon). For endothelial cells, rat anti-*CD31* antibody (BD Biosciences) was used, followed by goat anti-rat Alexa 594 (Invitrogen). For macrophages, rat anti-CD68 (Serotec) was used, followed by goat anti-rat Alexa 594 (Invitrogen). Slides were rinsed in PBS and mounted with ProLong Gold antifade reagent (P-36931; Invitrogen). Sections that had been stained by standard H&E (Merck) were examined to identify necrotic areas.

Image acquisition, processing, and analysis. Immunofluorescent images from each tumor section were captured with the use of an external digital camera (DXM-1200C; Nikon) on a Nikon fluorescence microscope (Nikon Eclipse TE 2000-S). Scanning at ×100 magnification yielded composite images of endothelial cells with the perfusion marker and pimonidazole with TAMs. Composite images were obtained at ×200 or ×630 magnification.

The images were analyzed by Image-Pro version 4 software (MediaCybernetics). Microvascular density (MVD) was determined as the number of pixels positive for *CD31* divided by the total tumor area. Regions of gross necrosis were visually selected on the H&E images and were outlined with a multiple-area-of-interest tool to determine the percentage in total tumor area. The hypoxia fraction was defined as the area positive for pimonidazole divided by the total tumor area (necrosis excluded). The density of macrophages in the hypoxic region was defined as the fraction of pixels positive for CD68 in the pimonidazole-positive tumor area divided by the fraction of total CD68+ pixels within the selected field.

Statistics. Data are presented as means with standard deviation. Statistical analyses used GraphPad Prism version 3 (GraphPad Software). For all comparisons, assessment of statistical significance was by unpaired t tests with significance set at $P \leq 0.05$.

Results

Reduction of tumor MVD after SD and fractionated-dose RT. Large SD (25 Gy) and MF (4 Gy per fraction × 5 days per

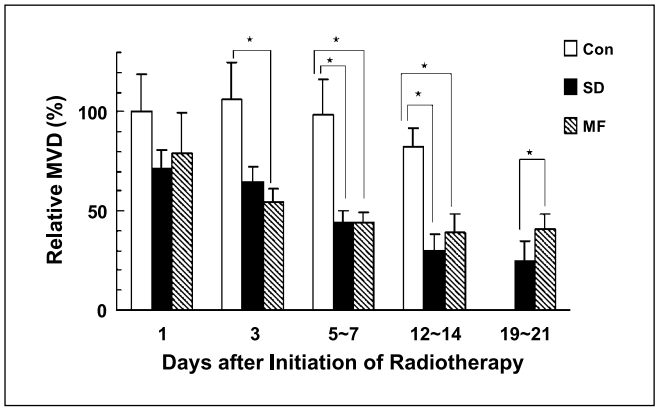

Fig. 1. The changes in MVD in TRAMP-C1 tumors after sham (control), SD, and MF RT. MVD was defined by the *CD31*+ area as a percent of the total tumor in the field of view. MVD of control tumors at 1 d before RT was used as reference level for comparisons. The corresponding tumor diameter of control tumors at days 1, 3, 7, and 14 was 4.3, 7, 10.6, and 13.2 mm, respectively. Bar, SE of 5 fields (non-necrotic areas) of 3 to 6 tumors for each time point. *, $P < 0.05$ by unpaired t test.

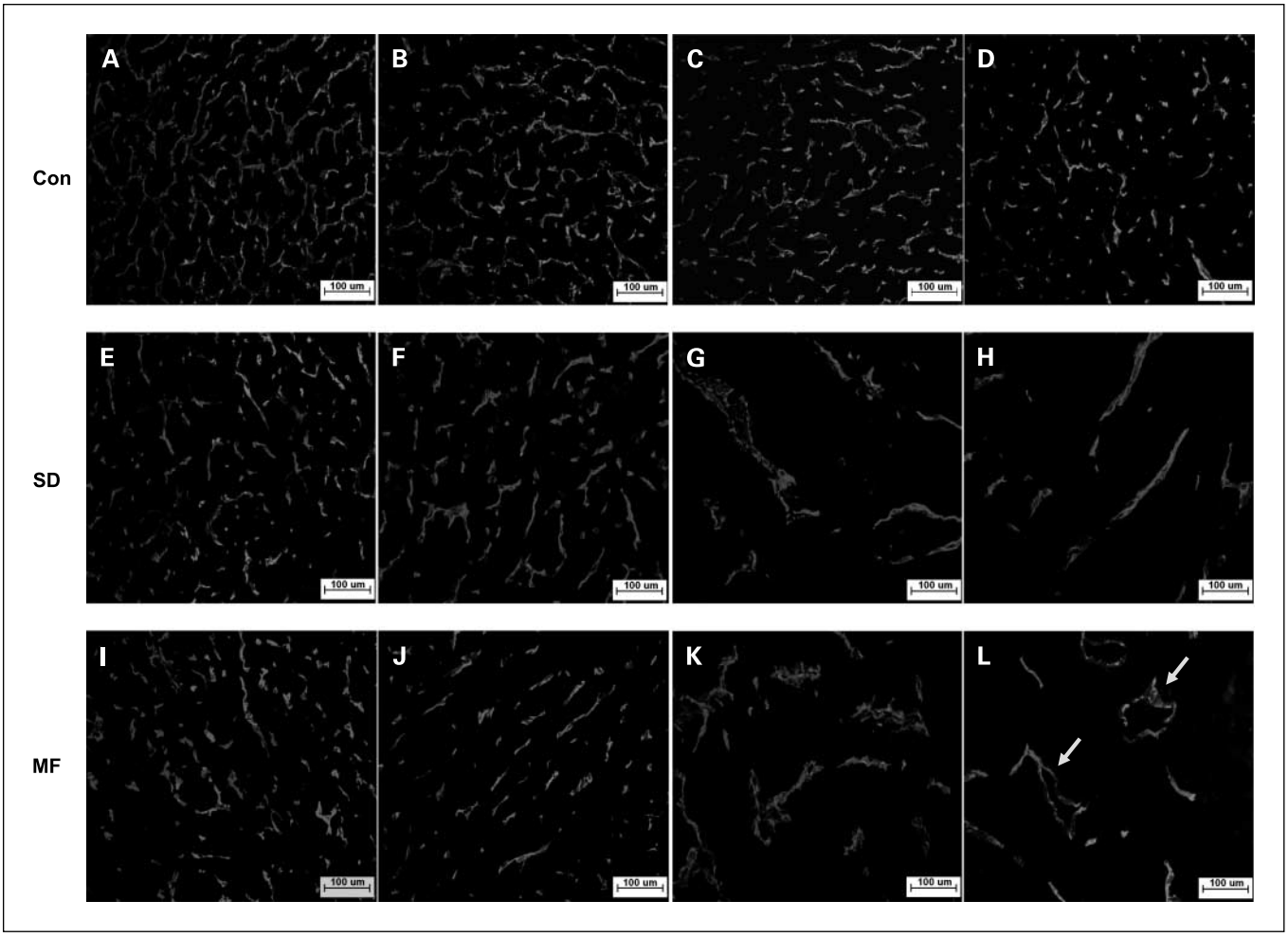

Fig. 2. The morphologic changes of TRAMP-C1 tumor vasculature after sham (control), SD, and MF RT. Endothelial cells were stained by anti-*CD31* antibody (*shown in white here*). Control tumors had relatively well-organized branching vessels (*A-D*; days 1, 3, 7, and 14). This well-organized structure was disrupted by either SD (*E-H*; days 1, 7, 14, and 21) or MF RT (*I-L*; days 1, 5, 12, and 19). The remaining vessels in the irradiated tumors at 3 wk were dilated with little or no branching; this is even more obvious in MF-irradiated tumors (*l, arrows*). Bar, 100 μm.

week × 3 weeks) doses were chosen because both caused ~1-week tumor growth delay. The effect on tumor MVD was compared with control tumors, with 1 day before irradiation as the reference point. As shown in Fig. 1, MVD remained relatively constant in control tumors until the tumors were larger than 10.6 mm. For SD irradiation, the MVD decreased to 71% ± 9% of reference levels at 1 day ($P > 0.05$) and progressively thereafter to 25% ± 9% at 3 weeks ($P < 0.05$). For MF, the MVD similarly decreased. Surprisingly, this was the case even 1 day after the first dose of 4 Gy (MVD, 79% ± 20%). Further decreases to 54% ± 7% at day 3 ($P < 0.05$) and around 40% from day 5 to day 19 ($P < 0.05$) were observed.

Alterations in vascular morphology and expression of angiogenesis-associated markers in irradiated tumors. Staining for endothelial cells showed that the microvasculature in control tumors was organized in a network. (Fig. 2A-D) As tumors grew, the distance between vessels and the diameter of vessels increased, which may explain why the MVD did not change too much with time (Fig. 1). As early as 1 day after either SD or MF irradiation, there was loss of capillary-like vessels (Fig. 2E and I) that became more obvious with time (Fig. 2E-L) so that at 3 weeks, most of the surviving vessels were relatively large (Fig. 2H and L). Subjectively, the vessels in MF-irradiated tumors seemed more dilated than those receiving SD. Interestingly, vessel perfusion assessed by the presence of Hoechst 33342 dye was less in irradiated than in control tumors (Supplementary Fig. S1).

To verify if these histologic changes were reflected in the expression of angiogenesis-associated factors, RNase protection assay was done (Fig. 3A-C). The TRAMP-C1 cell line cultured *in vitro*, used as control, had high levels of vascular endothelial growth factor (VEGF) and thrombin receptor, and moderate levels of VEGF-C (Fig. 3A, *column 1*). Thrombin receptors and VEGF have been associated with angiogenesis, and VEGF-C is required for the initial steps in lymphatic development (24). TRAMP-C1 tumors *in vivo*, in addition to what was found *in vitro*, expressed flt-1, flt-4, Tie, *CD31*, and *endoglin* (Fig. 3A), which were presumed to be host-cell derived. Although mRNA levels varied slightly between tumors at the same time point, VEGF and thrombin receptor expression in control tumors remained relatively constant with tumor growth although VEGF-C may have initially been high and decreased slightly with time (Supplementary Fig. S2), and this did not change after SD or MF RT (Supplementary Fig. S2). On the other

hand tie, *CD31*, and *endoglin* mRNA levels were significantly decreased 1 day after SD or MF RT (Fig. 3D; Supplementary Fig. S2). The same trend was noticed for *flt-4* although statistical significance was not reached. These results, put together, suggest that both RT schemes decrease the relative expression level of host-derived angiogenic factors, which is consistent with the decrease in MVD in irradiated tumors.

Irradiated tumors have less necrosis in a different distribution pattern. Although irradiated tumors had a progressive decrease in MVD, they continued to grow after a 1-week delay, raising the question of whether necrosis was increasing. Unexpectedly, less necrosis was evident in irradiated tumors (Fig. 4A). One week after RT, the percentage of necrosis decreased to 2% ± 2.8% and 2.8% ± 2.0% for SD-treated and MF-treated tumors, respectively, compared with 31% ± 6.8% for control. The corresponding figures were 14.7% ± 6.3%, 6.4% ± 5.7%, and 51.2% ± 16%, respectively, for tumors at 2 weeks after RT. The percentage increased slightly to 25.7% ± 8.3% (SD) and 11% ± 5.6% (MF) at 3 weeks after RT but was still lower than for control tumors at 2 weeks (51.2% ± 16%). Furthermore, the distribution of necrosis differed after RT. As shown in Fig. 4B, necrosis (delineated by the yellow line) in control tumors was in large continuous zones whereas in irradiated tumors it was in small, randomly distributed sites.

The relationship between hypoxia and vasculature. Because hypoxia is possibly one cause of necrosis, the relationship between these phenomena was examined. Pimonidazole staining for hypoxic regions in control tumors showed that the microvasculature was not perfused with Hoescht dye unlike the vasculature in nonhypoxic areas (Fig. 5A-a; Supplementary Fig. S1). Three weeks after RT, the vasculature in the hypoxic areas had disappeared (Fig. 5A-b and c) and areas of central necrosis were evident. We interpret this as RT eliminating the microvasculature associated with acutely hypoxic regions, making such regions chronically hypoxic. The change from transient to chronic hypoxia after RT was further supported by staining for carbonic anhydrase IX (Supplementary Fig. S1), which is a long-lived hypoxia-inducible factor–inducible endogenous protein. Carbonic anhydrase IX was highly expressed after RT but not in control tumors.

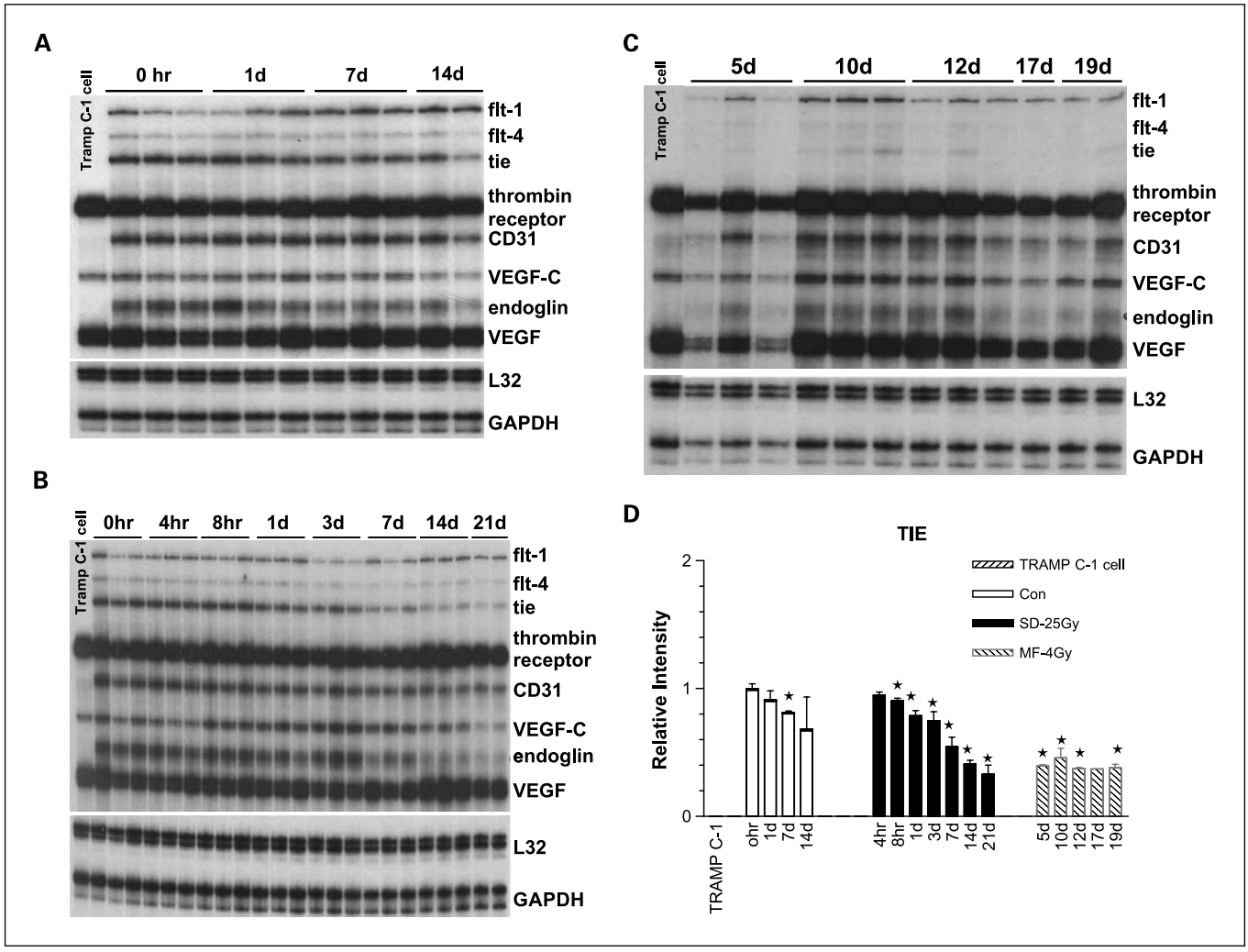

Fig. 3. A representative RNase protection assay showing expression of angiogenesis-associated genes in TRAMP-C1 tumors after RT. The probe set is a mAngio-1 Multi-Probe Template set from the BD RiboQuant system. L32 and glyceraldehyde-3-phosphate dehydrogenase housekeeping genes were used as loading controls. *A,* control tumors; *B,* SD-irradiated tumors; *C,* MF-irradiated tumors. The relative change of a representative angiogenic factor, tie, was calculated and plotted in *D*. The relative changes of other genes can be found in Supplementary Fig. S2. Bar, SE of 3 mice in the same plate. *, $P < 0.05$ by unpaired t test.

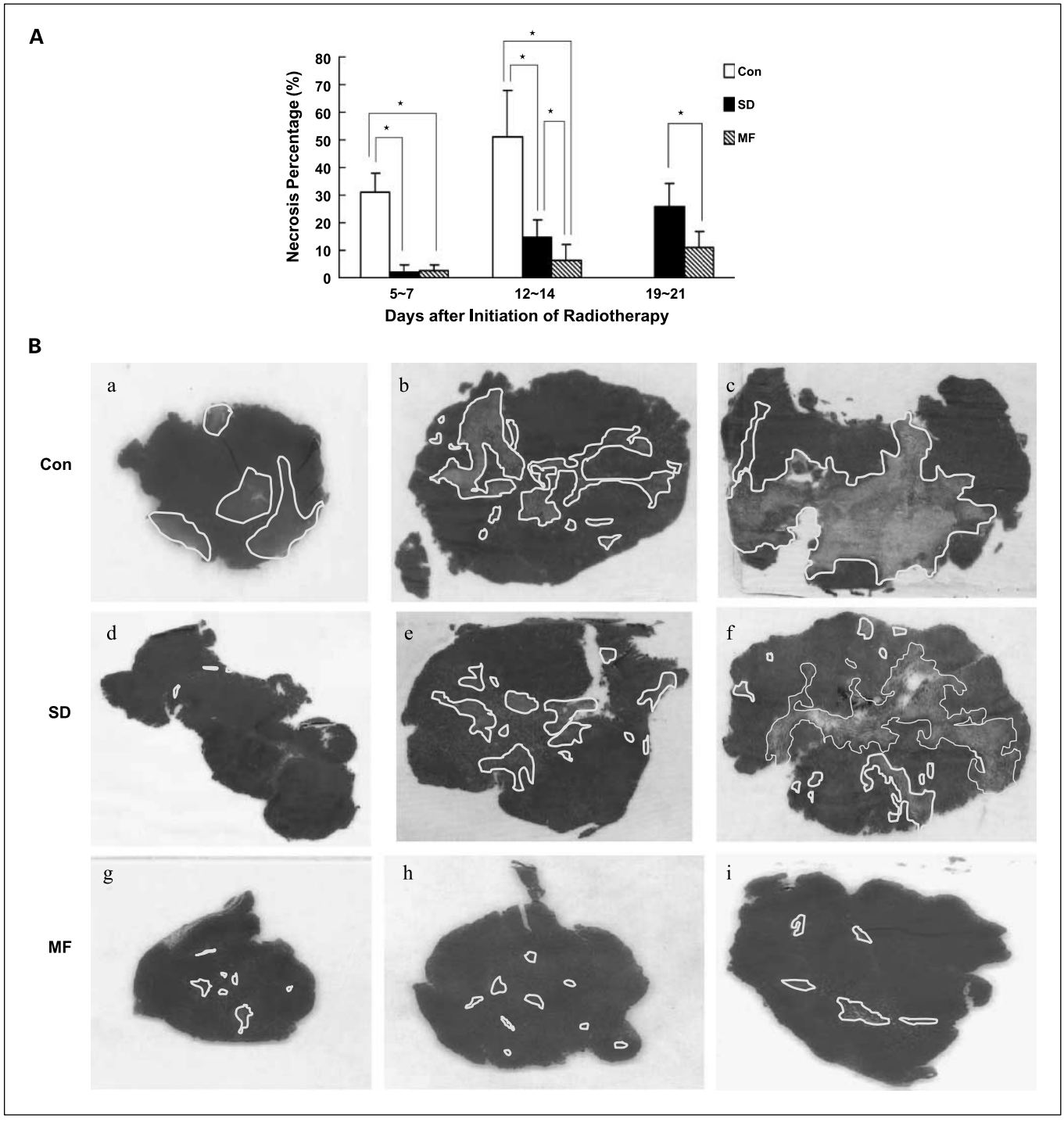

Fig. 4. *A,* percent necrosis in TRAMP-C1 tumors after sham (control), SD, and MF RT. The largest cross section of the tumor by H&E staining was used to calculate necrosis percentage. Bar, SE of 5 to 10 tumors at each time point. *, $P < 0.05$ by unpaired *t* test. *B,* necrosis. Necrosis, delineated by the white outline, in control tumors was as large continuous zones (*a-c*; 3, 7, and 14 d). SD-irradiated (*d-f*; 7, 14, and 21 d) and MF-irradiated (*g-i*; 5, 12, and 19 d) tumors had small and randomly distributed areas of necrosis whereas large SD-irradiated tumors (*e*; 21 d) had a pattern in between control and MF-irradiated tumors.

The percent of tumor hypoxia (Fig. 5B) did not significantly change at 1 day after SD or MF RT but was decreased at later time points. There did seem to be differences between SD and MF treatments. The latter remained fairly constant with time whereas the former increased late in the response. This presumably reflects continuing reoxygenation during the MF course.

TAMs aggregate in chronic hypoxic regions after RT. TAMs were shown to be attracted to and anchored at hypoxic regions by responding to expressed chemokines and cytokines (17, 25). Because they could be a major source of cytokines, we investigated their spatial location after RT. In contrast to Lewis' report on breast and cervical cancer models (10, 19), we did not see any particular spatial relation between CD68+ TAMs and

hypoxia in control tumors, in which they were randomly distributed throughout hypoxic and nonhypoxic regions (Fig. 6A). This pattern did not change over the 1st week after RT. However, at 2 weeks CD68+ TAMs started to aggregate in the developing chronic hypoxic regions. This was even more obvious at 3 weeks after both SD and MF RT (Fig. 6B and C). The degree of colocalization of CD68+ TAM with pimonidazole staining at 3 weeks after RT was calculated and plotted in Fig. 6D. The densities of CD68+ TAMs were significantly increased in hypoxic regions within both SD-irradiated and MF-irradiated tumors (both $P < 0.05$ by unpaired t test) but was more prominent in the former ($P < 0.05$).

Discussion

This study describes important microenvironmental changes after SD or MF RT. After either schedule, the MVD decreased from day 1 to week 3 to ~30% to 40% of that in control tumors. RT has been shown to induce apoptosis in endothelial cells *in vitro* (4) and *in vivo* (5) as early as 24 hours after exposure. We also detected apoptosis in endothelial cells in TRAMP-C1 tumors at 24 hours after SD RT (data not shown), and this can explain the rapid drop in MVD. What was more surprising was the persistence of this loss even when tumor growth resumed ~7 days after RT. A similar decrease has been reported in MVD at 14 days, but not 1 day, after a single dose of 12 Gy RT or an equivalent dose of fractionated RT to K1735 melanoma tumors (5) even though the authors did see endothelial cell apoptosis at day 1. The authors suggested that the late decrease in MVD was caused by ineffective angiogenesis (5). Our mRNA data suggest that decreased expression of host proangiogenic, endothelial-associated factors may be the cause of persistently low MVD levels and also supports the concept that the loss in vasculature is the result of impotent attempts at angiogenesis by a radiation-compromised endothelium.

The increase in diameter of the remaining vessels after RT has also been observed before (5). The reason is unknown, but our previous study showed progressive increases of mRNA levels of inducible nitric oxide synthase in irradiated tumors (21), and low levels of inducible nitric oxide synthase may produce sufficient nitric oxide to maintain the dilator tone and increase blood flow in tumor vessels (26, 27).

Pericytes are another principal cell in the blood vessel walls. These embed within the vascular basement membrane to form an outer sheath surrounding the endothelium (28) and regulate the formation, stabilization, remodeling, and function of the vasculature (29). In poorly differentiated prostate cancers from TRAMP mice, pericytes were abnormally shaped, variable in size, loosely associated with vessels, and had coverage that was not uniform (30). The vascular pattern in control tumors was very different from the large vessels remaining after RT, which were less torturous and had closely bound pericytes (Supplementary Fig. S3). This implies that these remaining vessels

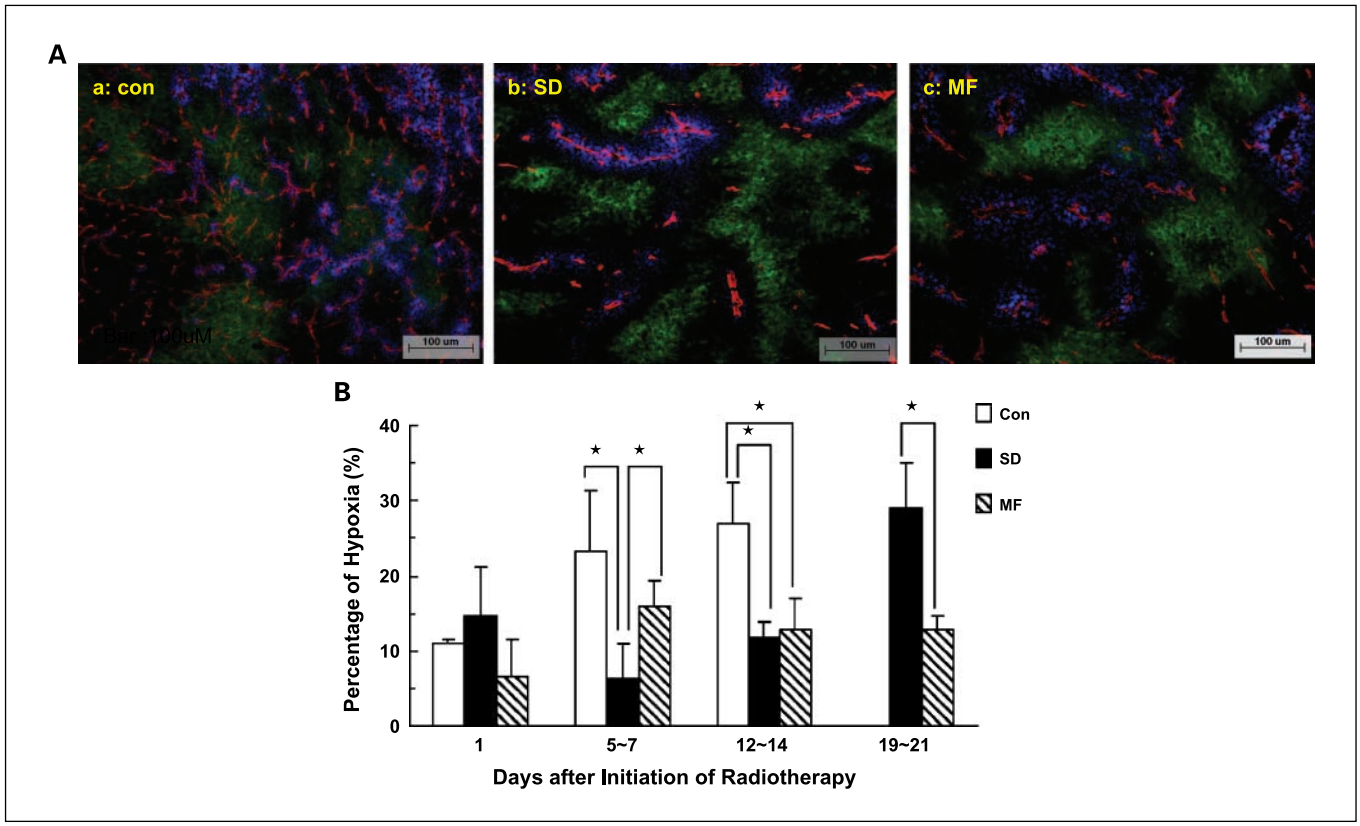

Fig. 5. *A,* the distribution of hypoxia, vasculature, and vascular perfusion in sham-irradiated (control; day14), SD-irradiated (day 21), and MF-irradiated (day 19) tumors. The hypoxic regions in control tumors were vascularized (*a*; con) but were not perfused by Hoechst 33342. There was almost no vasculature in the hypoxia regions of irradiated tumors (*b*, SD; *c*, MF). Green, pimonizadole stain for hypoxia; red, *CD31* stain for endothelial cells; blue, Hoechst 33342 for vascular perfusion. Bar, 100 μm. *B,* the change in hypoxia fraction after SD or MF RT is shown as a histogram. Tumor samples after MF RT were taken 2 d earlier than control and SD-RT tumors to account for the MF schedule. Bar, SE of 3 to 6 tumors for each time point. *, $P < 0.05$ by unpaired t test.

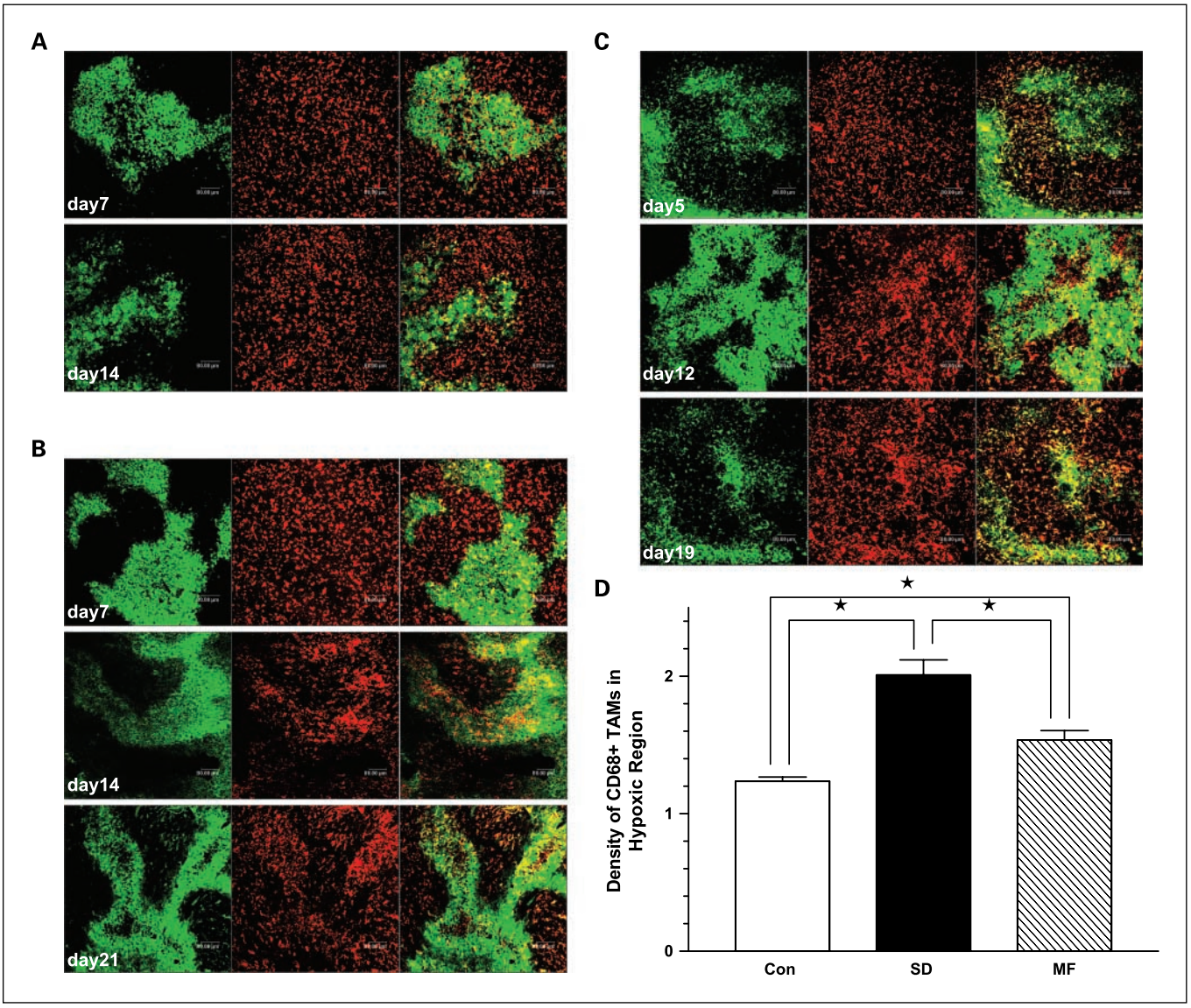

Fig. 6. The distribution of hypoxia and CD68+ TAMs in control (*A*), SD-irradiated (*B*), and MF-irradiated (*C*) tumors at different times after the initiation of RT. Green, anti-pimonizadole stain for hypoxia regions; red, anti-CD68 antibody for TAMs. Merged images, the colocolization of hypoxia and TAMs. The density of CD68+ TAMs in the hypoxic region is plotted in a histogram (*D*). Bar, SE of 5 fields of 5 tumors. *, $P < 0.05$ by unpaired *t* test. Bar, 80 μm.

might be less permeable and more efficient in supplying blood and nutrients to surrounding tumor cells.

Our data suggest that RT retards angiogenesis; however, tumors regrow very effectively. The decrease of the expression of endothelial cell marker genes, such as *CD31*, *endoglin*, Tie, and *Flt-4* after RT is in keeping with their radiation-induced death. Loss of *endoglin*, a transforming growth factor-β binding protein, causes poor vascular smooth muscle development and arrested endothelial remodeling (31). Decreased expression of Flt-4, which functions at sprouting first lymphatic vessels from embryonic veins, has been associated with pathologic angiogenesis (24, 32) and contributes to the debranched phenomena in irradiated tumors. Whereas biological targeting of neovascularization is popular, with and without RT, our study clearly indicates that angiogenesis may not be a major factor determining tumor regrowth after RT.

Microvessels within hypoxic regions of control tumors were presumably functionally inefficient because many of them were not perfused by Hoechst dye. Such areas may be presumed to be acutely hypoxic, which is supported by the lack of carbonic anhydrase IX expression, a marker associated with cells exposed to diffusion-limited chronic hypoxia over a long time period (33). Remarkably, nearly no microvessels were found in the hypoxic regions of irradiated tumors at 2 to 3 weeks, suggesting chronic hypoxia caused by vascular deficiency predominated. This conclusion was supported by carbonic anhydrase IX staining. This seems to suggest that the acutely hypoxic microvasculature is relatively sensitive to irradiation. This may be as a result of the induction of a p53-dependent proapoptotic phenotype by hypoxia (34, 35) that might selectively radiosensitize endothelium in this area.

Reoxygenation during RT is an advantage for fractionated treatment, and we showed that RT decreased the percentage of

hypoxia after 1 week but not after 1 day. The hypoxic fraction of SD-irradiated tumors gradually increased to control levels as tumors regrew, but this was not true for MF RT, suggesting that there is reoxygenation during and/or after RT and that MF RT prolongs this reoxygenation. More interesting was that there was an apparent shift from transient to chronic hypoxia at 2 to 3 weeks even after MF RT. This suggests a changing target for therapeutic strategies aimed at hypoxic cells even at later phases of a MF RT regimen.

One perhaps surprising finding from our study was that irradiated tumors had a lower percentage of necrosis than control tumors in spite of vascular loss, with the lowest values in MF-treated tumors. Moreover, the necrosis was more dispersed and located in the center of a region of chronic hypoxia after RT. Control tumors, on the other hand, usually had a large area of central necrosis. The fact that necrosis was linked to the development of small, diffuse avascularized areas of chronic hypoxia again indicates the dynamic nature of the changes in the tumor microenvironment after RT.

TAMs are a major cellular component of human (36) and murine cancers (37, 38). They can accumulate in hypoxic regions (10, 19), and their number in these regions correlates with poor prognosis in several human cancers (14, 15, 39, 40). Remarkably, CD68+ TAMs, which were randomly distributed in unirradiated tumors and not associated with hypoxic regions, began to accumulate in hypoxia regions after RT, coincident with the development of the avascularized chronic hypoxic regions.

Chronic hypoxia is known to produce macrophage chemoattractants, such as endothelial monocyte–activating polypeptide II, endothelin 2, and VEGF (10), to trigger TAM migration, which may form a depot for cytokine release that may promote an avalanche of endothelial cell death and impotent attempts at angiogenesis. We have shown previously that TAMs from irradiated TRAMP-C1 tumors expressed higher level of inducible nitric oxide synthase (21) at 2 to 3 weeks, the time of accumulation of TAMs in hypoxic regions. Nitric oxide generated from TAMs of irradiated tumors can increase hypoxia-inducible factor–1α expression (41), which regulates >60 genes that are involved in angiogenesis, metabolism, cell death, and metastasis (42). These TAMs also express higher levels of arginase I and cyclooxygenase-2, which may contribute to enhanced tumor growth and proliferation after RT (21). TAMs within chronically hypoxic areas that develop would be prime targets for modulating tumor responses after RT.

In summary, we have shown in at least this murine prostate cancer model that RT can cause a shift from acute to chronic hypoxia by eliminating microvasculature in acutely hypoxic areas. The chronic hypoxia that develops becomes associated with TAMs that may form a depot for cytokines that dictate tumor regrowth even at the same time as vascular collapse leading to necrosis. This changing microenvironmental landscape after RT, if verified in human tumors, will need to be taken into account when targeting vasculature and/or hypoxia with therapeutic intent.

Disclosure of Potential Conflicts of Interest

No potential conflicts of interest were disclosed.

Acknowledgments

We thank Ching-Jung Lo, Yi-Chen Liu, Chin-Yi Lee, and Chih-Chun Chen of the Confocal Microscopy Core Facility of the Chang Gung Memorial Hospital for help in dosimetry verification, mouse irradiation, processing of samples, and technical matters.

References

1. Trott KR. Tumour stem cells: the biological concept and its application in cancer treatment. Radiother Oncol 1994;30:1–5.
2. Hendry JH, West CM, Moore JV, Potten CS. Tumour stem cells: the relevance of predictive assays for tumour control after radiotherapy. Radiother Oncol 1994;30:11–6.
3. Folkman J. Anti-angiogenesis: new concept for therapy of solid tumors. Ann Surg 1972;175:409–16.
4. Ahmad M, Khurana NR, Jaberi JE. Ionizing radiation decreases capillary-like structure formation by endothelial cells *in vitro*. Microvasc Res 2007;73:14–9.
5. Tsai JH, Makonnen S, Feldman M, Sehgal CM, Maity A, Lee WM. Ionizing radiation inhibits tumor neovascularization by inducing ineffective angiogenesis. Cancer Biol Ther 2005;4:1395–400.
6. Lorke DE, Wenzel S, Siebert K, Zywietz F. Microvascular and tumor cell alterations during continuous hyperfractionated irradiation: an electron microscopic investigation on the rat R1H rhabdomyosarcoma. Int J Radiat Oncol Biol Phys 1999;44:895–904.
7. Garcia-Barros M, Paris F, Cordon-Cardo C, et al. Tumor response to radiotherapy regulated by endothelial cell apoptosis. Science 2003;300:1155–9.
8. Moeller BJ, Dreher MR, Rabbani ZN, et al. Pleiotropic effects of HIF-1 blockade on tumor radiosensitivity. Cancer Cell 2005;8:99–110.
9. Fuks Z, Kolesnick R. Engaging the vascular component of the tumor response. Cancer Cell 2005;8:89–91.
10. Murdoch C, Giannoudis A, Lewis CE. Mechanisms regulating the recruitment of macrophages into hypoxic areas of tumors and other ischemic tissues. Blood 2004;104:2224–34.
11. Mantovani A, Sozzani S, Locati M, Allavena P, Sica A. Macrophage polarization: tumor-associated macrophages as a paradigm for polarized M2 mononuclear phagocytes. Trends Immunol 2002;23:549–55.
12. Lin EY, Li JF, Gnatovskiy L, et al. Macrophages regulate the angiogenic switch in a mouse model of breast cancer. Cancer Res 2006;66:11238–46.
13. Dirkx AE, Oude Egbrink MG, Wagstaff J, Griffioen AW. Monocyte/macrophage infiltration in tumors: modulators of angiogenesis. J Leukoc Biol 2006;80:1183–96.
14. Leek RD, Lewis CE, Whitehouse R, Greenall M, Clarke J, Harris AL. Association of macrophage infiltration with angiogenesis and prognosis in invasive breast carcinoma. Cancer Res 1996;56:4625–9.
15. Hanada T, Nakagawa M, Emoto A, Nomura T, Nasu N, Nomura Y. Prognostic value of tumor-associated macrophage count in human bladder cancer. Int J Urol 2000;7:263–9.
16. Murdoch C, Lewis CE. Macrophage migration and gene expression in response to tumor hypoxia. Int J Cancer 2005;117:701–8.
17. Lewis C, Murdoch C. Macrophage responses to hypoxia: implications for tumor progression and anticancer therapies. Am J Pathol 2005;167:627–35.
18. Luo Y, Zhou H, Krueger J, et al. Targeting tumor-associated macrophages as a novel strategy against breast cancer. J Clin Invest 2006;116:2132–41.
19. Lewis CE, Pollard JW. Distinct role of macrophages in different tumor microenvironments. Cancer Res 2006;66:605–12.
20. Biswas SK, Sica A, Lewis CE. Plasticity of macrophage function during tumor progression: regulation by distinct molecular mechanisms. J Immunol 2008;180:2011–7.
21. Tsai CS, Chen FH, Wang CC, et al. Macrophages from irradiated tumors express higher levels of iNOS, arginase-I and COX-2, and promote tumor growth. Int J Radiat Oncol Biol Phys 2007;68:499–507.
22. Foster BA, Gingrich JR, Kwon ED, Madias C, Greenberg NM. Characterization of prostatic epithelial cell lines derived from transgenic adenocarcinoma of the mouse prostate (TRAMP) model. Cancer Res 1997;57:3325–30.
23. Hong JH, Chiang CS, Campbell IL, Sun JR, Withers HR, McBride WH. Induction of acute phase gene expression by brain irradiation. Int J Radiat Oncol Biol Phys 1995;33:619–26.
24. Karkkainen MJ, Haiko P, Sainio K, et al. Vascular endothelial growth factor C is required for sprouting of the first lymphatic vessels from embryonic veins. Nat Immunol 2004;5:74–80.
25. Murdoch C, Muthana M, Lewis CE. Hypoxia regulates macrophage functions in inflammation. J Immunol 2005;175:6257–63.
26. Fukumura D, Yuan F, Endo M, Jain RK. Role of nitric oxide in tumor microcirculation. Blood flow, vascular permeability, and leukocyte-endothelial interactions. Am J Pathol 1997;150:713–25.

27. Andrade SP, Hart IR, Piper PJ. Inhibitors of nitric oxide synthase selectively reduce flow in tumor-associated neovasculature. Br J Pharmacol 1992;107:1092–5.
28. Risau W. Mechanisms of angiogenesis. Nature 1997;386:671–4.
29. Armulik A, Abramsson A, Betsholtz C. Endothelial/pericyte interactions. Circ Res 2005;97:512–23.
30. Ozawa MG, Yao VJ, Chanthery YH, et al. Angiogenesis with pericyte abnormalities in a transgenic model of prostate carcinoma. Cancer 2005;104:2104–15.
31. Li DY, Sorensen LK, Brooke BS, et al. Defective angiogenesis in mice lacking *endoglin*. Science 1999;284:1534–7.
32. Dumont DJ, Jussila L, Taipale J, et al. Cardiovascular failure in mouse embryos deficient in VEGF receptor-3. Science 1998;282:946–9.
33. Ljungkvist AS, Bussink J, Kaanders JH, van der Kogel AJ. Dynamics of tumor hypoxia measured with bioreductive hypoxic cell markers. Radiat Res 2007;167:127–45.
34. Greijer AE, van der Wall E. The role of hypoxia inducible factor 1 (HIF-1) in hypoxia induced apoptosis. J Clin Pathol 2004;57:1009–14.
35. Koumenis C, Alarcon R, Hammond E, et al. Regulation of p53 by hypoxia: dissociation of transcriptional repression and apoptosis from p53-dependent transactivation. Mol Cell Biol 2001;21:1297–310.
36. van Ravenswaay Claasen HH, Kluin PM, Fleuren GJ. Tumor infiltrating cells in human cancer. On the possible role of CD16+ macrophages in antitumor cytotoxicity. Lab Invest 1992;67:166–74.
37. McBride WH, Moore K. The effect of C. parvum therapy on intratumoral macrophage subpopulations. Adv Exp Med Biol 1982;155:731–6.
38. Milas L, Wike J, Hunter N, Volpe J, Basic I. Macrophage content of murine sarcomas and carcinomas: associations with tumor growth parameters and tumor radiocurability. Cancer Res 1987;47:1069–75.
39. Salvesen HB, Akslen LA. Significance of tumour-associated macrophages, vascular endothelial growth factor and thrombospondin-1 expression for tumour angiogenesis and prognosis in endometrial carcinomas. Int J Cancer 1999;84:538–43.
40. Lissbrant IF, Stattin P, Wikstrom P, Damber JE, Egevad L, Bergh A. Tumor associated macrophages in human prostate cancer: relation to clinicopathological variables and survival. Int J Oncol 2000;17:445–51.
41. Li F, Sonveaux P, Rabbani ZN, et al. Regulation of HIF-1α stability through S-nitrosylation. Mol Cell 2007;26:63–74.
42. Semenza GL. Targeting HIF-1 for cancer therapy. Nat Rev Cancer 2003;3:721–32.